J Appl Electrochem (2008) 38:679–687
DOI 10.1007/s10800-008-9487-5

ORIGINAL PAPER

Influence of surface roughness on the semiconducting properties of oxide films formed on 304 stainless steel

N. E. Hakiki

Received: 13 February 2007 / Revised: 21 December 2007 / Accepted: 18 January 2008 / Published online: 5 February 2008
© Springer Science+Business Media B.V. 2008

Abstract Oxide films were formed at 350 °C in borate buffer solution on AISI 304 stainless steel priory abraded with wet SiC paper of different grit size. The films were characterised by Atomic Force Microscopy (AFM) and studied by capacitance, impedance, and photocurrent measurements. The images obtained by AFM microscopy show the evolution of the surface roughness of the films with increasing grit size. Capacitance measurements show that, in all cases, the electronic structure of the films is comparable to that of a p–n heterojunction. This structure is due to the development of space charge layers in the outer iron oxide region at the film/electrolyte interface and in the inner chromium oxide region at the film/metal interface. However, donor and acceptor densities are closely related to the surface roughness via the grit size of the wet SiC paper. An increase in capacitance leading to higher doping densities is manifested by an increase in grit size. These parameters are also frequency dependent. An investigation of the frequency dispersion in relation to the evolution of the surface roughness was performed by analysing the Bode plots through the impedance measurements. The photocurrent results, obtained for the oxide films formed on the different abraded AISI 304, show an increasing photoresponse with decreasing grit size. In spite of this, a constant value of the band gap energy was obtained whatever the oxide film considered. The photocurrent response near the absorption edge is also discussed. The photocurrent response at fixed wavelength and as a function of the applied potential is also influenced by the grit size.

Keywords Oxide films · Grit size · Surface roughness · AFM microscopy · Capacitance · Impedance · Photocurrent

N. E. Hakiki (✉)
Laboratoire de Physique des Couches Minces et Matériaux pour l'Electronique, Faculté des Sciences, Université d'Oran, 31000 Oran, Algéria
e-mail: nour_hakiki@yahoo.fr

1 Introduction

The study of the properties of thick oxide films and very thin passive films formed on stainless steels is still of fundamental and practical importance in corrosion science. The film is best described as a highly doped graded structure; the closest classical analogue being an inverse exponentially doped tunnel diode [1]. However, a clear correlation between the film structure and its stability has never established since the exact electronic structure of these films is not fully known. In fact, many investigations have been performed on oxide and passive films formed in different environments on alloys containing iron, chromium and nickel, such as stainless steels and nickel based alloys demonstrating the semiconducting character of such films. In the literature, these studies have been performed by in situ techniques such as capacitance, impedance, and photocurrent measurements [2–27], giving valuable information about band gap energies, conductivity type and flat band potentials of the films. Using band theory, solid-state properties of these films formed in solution have been determined and correlated with their stability in some cases [5]. The oxide films formed on stainless steels and alloys generally present strong gradients of chemical composition and may comprise regions of different semiconductivity [4]. Under certain conditions, the electronic structure of the film can be more accurately described by a bilayer model composed of an internal chromium-rich oxide region,

which plays the major role in corrosion resistance and by an external iron-rich oxide region, which controls the electrochemical properties of the film/electrolyte interface. These two regions form a duplex structure of different chemical composition and semiconductivity type [6]. Both regions are highly doped and are therefore analogous to a tunnel diode, but here the films are n-type doped by Fe^{2+} [6, 13, 15]. Understanding the influence of the electronic structure of the passive and oxide films on the corrosion resistance of stainless steels implies the ability to describe, not only the space charges created at both metal/film and film/electrolyte interfaces, but also in the n–p heterojunction situated in the internal part of the film.

It has been established that the electronic structure of an anodically grown film on iron in borate buffer solution (pH = 8.4) can be described in terms of a duplex film with Fe_30_4 inner layer and a highly doped n-type Fe_2O_3 outer layer [25]. The influence of localized states and deep donor levels on photoelectrochemical [26] and capacitance results respectively [26, 27], has been shown and taken into account in the debate concerning the electronic structure of iron oxide. For ferritic stainless steel, the photoelectrochemical measurements carried out on anodically grown films in sulphate solution (pH = 6), show a possible simultaneous presence of iron and chromium oxide [7]. The photoelectrochemical response of stainless steel in the same environment shows that the anodic films are highly defective and that they possess a high number of localised states [16]. The non-stoichiometric compositions or the local structural inhomogeneities are cited as possible causes of these states.

In the case of thermally grown oxide films, it is assumed that the inner region consists of a mixed iron–chromium spinel oxide $(Fe^{3+}_{2-x}Cr^{3+}_{x}Fe^{2+})O^{2-}_{4}$ with $0 \leq x \leq 2$ [28]. The influence of temperature on film formation can be related to the value of x which increases when the temperature is decreased. The transport of iron ions in the inner layer competes with that of oxygen ions in the outer Fe_2O_3 layer in such a way that the lower the temperature of film formation is, the more the film formed is deficient in Fe^{3+}. The composition of the outer layer of the films can thus be described as an oxide containing Fe^{2+} and Fe^{3+} with the ratio Fe^{3+}/Fe^{2+} increasing with the temperature of film formation. This picture does not exclude the presence of some Cr^{3+} substituting Fe^{3+} ions in the oxide lattice, although this process is much more important for the inner layers of the film, as shown by analytical studies.

A number of investigations have been devoted to the identification of the oxide phases formed [29–41]. Results reveal the predominance of spinel oxides [33]. The motivation for this kind of investigation was the strong dependence of the protective character of the film on the nature of the oxide phases present. There have been relatively few investigations of the relationships between the composition, crystallographic structure, and electronic properties of the oxide film. Recent studies [40, 41] of films formed on AISI type 304 stainless steel and Alloy 600 in a primary type environment of a pressurised water reactor (PWR) show that there is a critical temperature at which the conductivity of the oxide film passes from n-type to p-type. The question remains: What is the type of conductivity that is particularly favourable to the development of stress cracking corrosion (SCC). Thus, further research is necessary to understand how the electronic structure of the oxide films causes or affects the SCC susceptibility. Furthermore, because the electronic structure itself must be affected by the defect structure, more detailed information about the crystallographic nature of the constituent oxides is required.

The purpose of this paper is to obtain more detailed information about the electronic structure of the films formed on AISI stainless steel with particular emphasis on the influence of the surface roughness, determined by AFM imaging. Capacitance, impedance, and photocurrent measurements are reported in order to further clarify the influence of the grit size of the abrading paper on the electronic structure of the oxide films formed on the alloy. The characterisation of the films using near field microscopy is complemented with additional electronic structure investigations using electrochemical techniques.

2 Experiments

Austenitic type AISI 304 stainless steel of composition (wt%) (Cr: 17.4, Ni: 8.3, C: 0.053, N: 004, Si: 0.48, Mn: 1.42, Mo: 0.39, Cu: 0.14) was used for the test specimens. The samples, of surface area 0.8 cm^2 were annealed for 1/2 h at 1050 °C. Then, they were abraded with wet SiC paper of different grit size, rinsed in distilled water, ultrasonically cleaned and dried in air. Oxidation of the samples was made in air at a controlled temperature of 350 °C in a furnace for 2 h at atmospheric pressure. AFM images were recorded using TOPMETRIX 2010 AFM-STM system. For electrochemical measurements, a classical cell with three electrodes was used with a platinum counter-electrode (area = 1 cm^2) and a saturated calomel electrode (SCE) as reference. All the experiments were carried out at room temperature (22 °C) under continuous high purity nitrogen bubbling in a buffer solution of composition H_3BO_3 (0.05 M) + $Na_2B_4O_7 \cdot 10H_2O$ (0.075 M) leading to pH = 9.2. The specimens previously oxidised were immersed in the solution and left at the rest potential for 2 h before measurements were taken. Polarisation was applied in successive steps of 50 mV in the

cathodic direction, starting from the rest potential. The polarisation time before each measurement was 10 s. A potentiostat (PAR 273) and a double phase synchronous detector (Brookdeal 5208 lock-in amplifier) with an internal oscillator working in a large frequency range 5 Hz–100 kHz were used. The principle of the experiment is to simultaneously apply a perturbing signal ΔU (10 mV r.m.s) to the cell via the potentiostat. The response is compared to ΔU dephased by $\Delta\phi + \pi/2$. At high frequencies, the capacitance can be calculated using the relation $C = (-Z_{im} \cdot 2\pi f)^{-1}$, where Z_{im} is the imaginary part of the impedance and f is the frequency. The capacitance measurements, corrected for the real electrode surface computed using Topometrix 2010 Software, were carried out at different frequencies in the potential range 1 to −1.5 V. Photoelectrochemical measurements were performed using a 150 W xenon lamp and a 1200/mm grating monochromator (Jobin Yvon H25). The photocurrents were generated by focusing the light with a fused silica lens through a quartz window of the electrochemical cell onto the working electrode. The lock-in technique allowed separation of the photocurrent from the passive current by chopping the light at a constant frequency (19 Hz) and feeding the signal as well as the current output of the potentiostat to the lock-in amplifier. The photocurrent spectra were obtained by scanning the wavelength of the light in steps of 50 nm from 750 to 250 nm. The dependence of the photocurrent on the applied potential was obtained at a fixed wavelength (350 nm) applying potential in the same way as in the capacitance measurements. The photocurrent action spectra were corrected for the lamp efficiency without taking into account the reflections at the film-solution interface and for the real electrode surface computed using the Topometrix 2010 Software.

3 Results and discussion

3.1 Surface imaging and roughness

Figure 1 presents AFM images of oxide films formed on AISI 304 stainless steel abraded with wet SiC paper of different grit size. It appears clearly that the film formed on substrate abraded with small grit size (1 μm) has a very small surface roughness (Fig. 1a, RMS value = 10 nm), and that the roughness increase with the grit size (Fig. 1b–d) until a value of 90 nm for a grit size of 46 μm. To be more quantitative, we determine the surface roughness parameter named RMS using the Topometrix 2010 Software as a function of the grit size of the wet SiC paper. The parameter RMS is calculated using the following expression:

$$\mathrm{RMS} = \sqrt{\frac{1}{512}\sum_{i=1}^{512}\left[h(x_i, y_i, t) - E_p(t)\right]^2} \quad (1)$$

with $E_p(t) = \frac{1}{512}\sum_{i=1}^{512} h(x_i, y_i, t)$ the mean height of the height distribution.

Figure 2 shows the dependence of surface roughness on increasing grit size. The RMS value increase slowly until a grit size of 15 μm, then an abrupt change in surface state occurs near 20 μm. For a grit size higher than 20 μm, the RMS value tends to a saturation value near 90 nm. Notice that the calculated roughness is the sum of two contributions, the roughness due to the oxidation process and the roughness due to the polishing process. For grit size up to 15 μm, the RMS factor is dominated by the grain-like morphology of the oxide layer, whereas at higher grit sizes the RMS value reflects mostly the stripes due to the polishing process. However, it appears also on Fig. 1 that the oxide grain shape is influenced by the density and thickness of the stripes. So, in this paper, we try to control the surface roughness using different grit sizes in order to understand its influence on the semi-conducting properties of the oxide layer as formed.

3.2 Open-circuit potential

The open-circuit potential attained after 2 h immersion in the borate buffer solution, by the oxide films formed at 350 °C on AISI 304 substrate abraded with wet SiC paper of different grit size is presented on Fig. 3. A continuous decrease in the open-circuit potential is manifested when the grit size increases. Comparing with Fig. 2, we notice that the decrease in open-circuit potential is related to the increase in surface roughness. This behaviour will be justified by the examination of capacitance results.

3.3 Capacitance measurements

Capacitance measurements performed in the higher potential range ($U > -0.5$ V) at 3160 Hz are represented in Fig. 4a showing the plot of capacity C^{-2} versus the applied potential U for oxide films formed at 350 °C on AISI 304 stainless steel for different grit size. The existence of typical Mott–Schottky linear variations with positive slope, which are representative of a semiconducting electrochemical behaviour of an n-type semiconductor, is evidenced. In the lower potential range ($U < -0.5$ V), the results are represented in Fig. 4b revealing the existence of typical Mott–Schottky linear variations with negative slope which are representative of a semiconducting electrochemical behaviour of a p-type

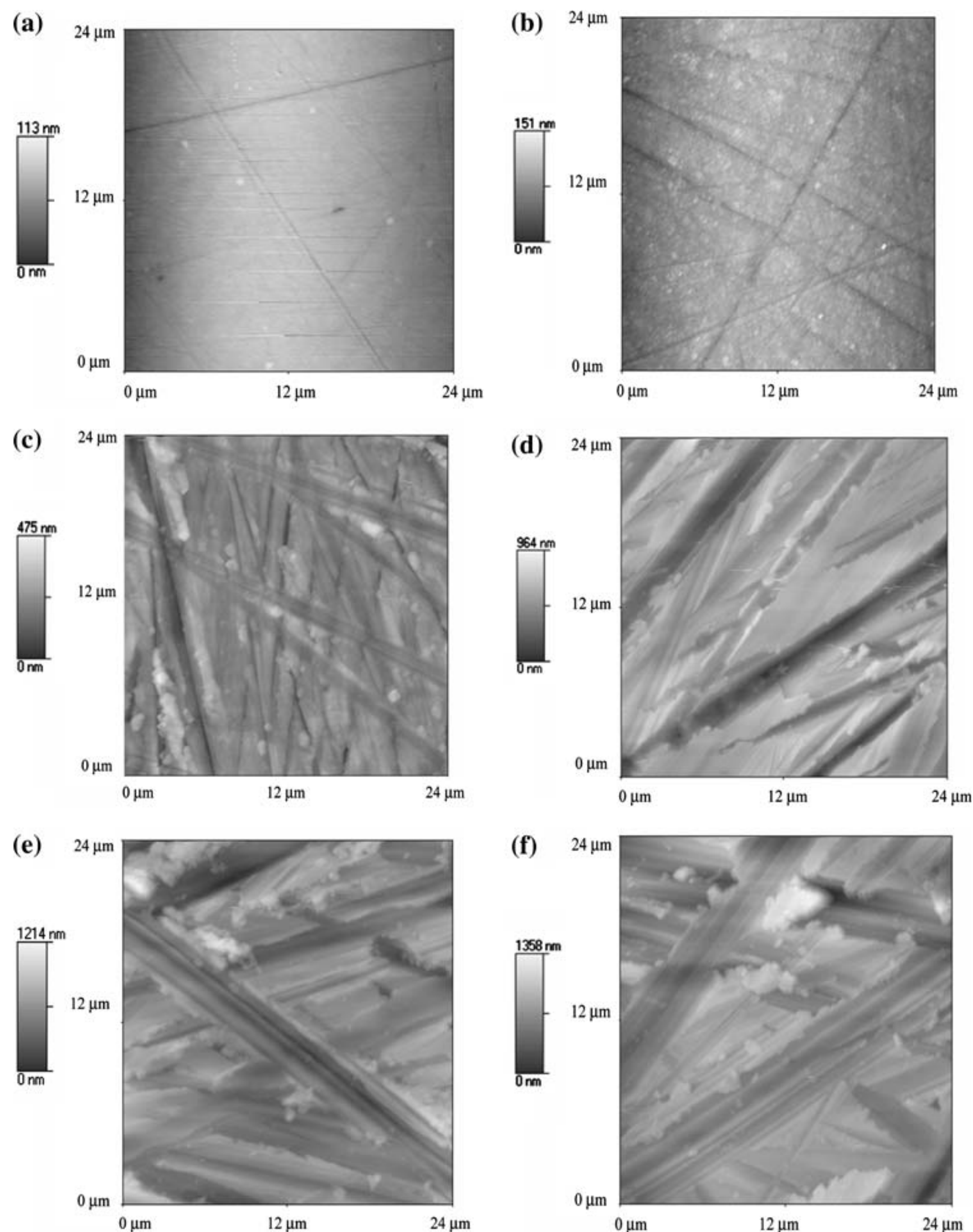

Fig. 1 AFM microscopy images of oxide films formed on AISI 304 stainless steel at 350 °C abraded with wet SiC paper of different grit size (**a**) 1 µm, (**b**) 5 µm, (**c**) 15 µm, (**d**) 22 µm, (**e**) 30 µm, (**f**) 46 µm

semiconductor. Such behaviour has recently been reported for films formed on iron [23–27] and stainless steels [2–22] and can be related to the fact that the capacitance response in the higher potential range ($U > -0.5$ V) represented in Fig. 4a is controlled by the electronic structure of the outer γ-Fe_2O_3 oxide layers having n-type semiconductor behaviour [23–27] and in the lower potential range ($U < -0.5$ V) represented in Fig. 4b by the electronic structure of the inner Cr_2O_3 oxide layers considered as a p-type semiconductor [18]. To explain such behaviour, account has to be taken of the concepts of band bending, well established in semiconductor physics and semiconductor electrochemistry. On the other hand, it is also necessary to consider that the capacitance measurements reflect the behaviour of a particular heterojunction where the development of space charge regions occurs at the film/metal and film/electrolyte interfaces. For thin passive films this heterojunction is formed by an inner region of chromium oxide with p-type semi-conductivity [18] and an outer region of iron oxide with n-type semiconductivity [2–6]. The amount of nickel oxide found in the films does not significantly influence the heterojunction. The chromium oxide acts as a Schottky barrier in the potential range where the iron oxide behaves as an ohmic contact and vice-versa [2–6]. The electronic band structure model proposed in previous work [2–6], demonstrates that the passive film acts as a Schottky barrier above and below the flat-band potential that is situated at about −0.5 V. It was shown that the semiconductive properties are related to the chemical composition of the films. Based on the capacitance results,

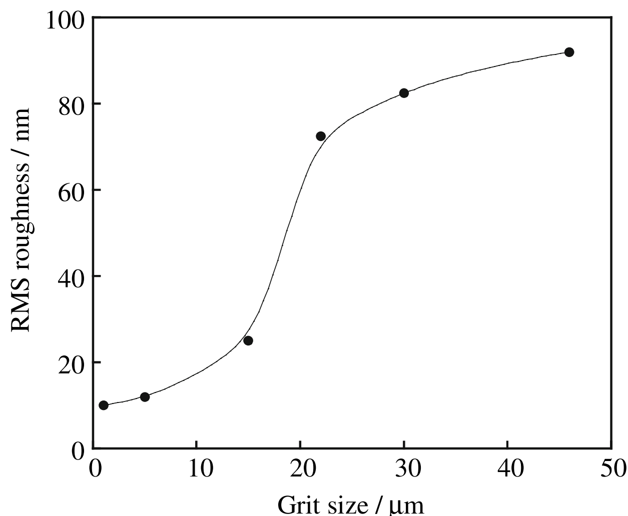

Fig. 2 Plot of RMS surface roughness versus grit size

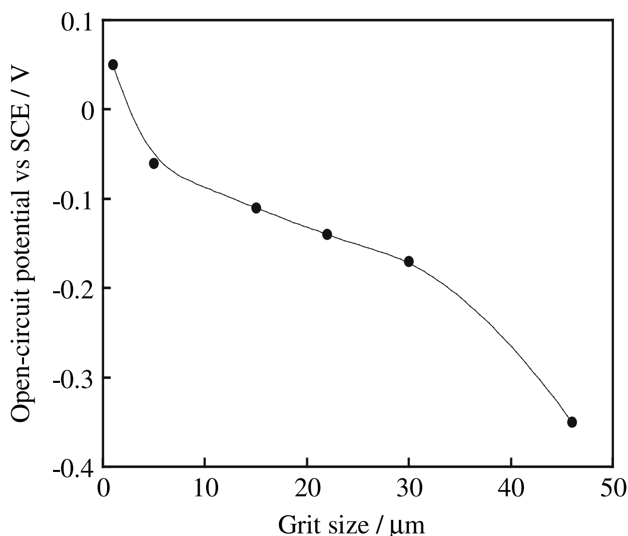

Fig. 3 Plot of open-circuit potential of AISI 304 stainless steel against grit size in borate buffer solution for 2 h

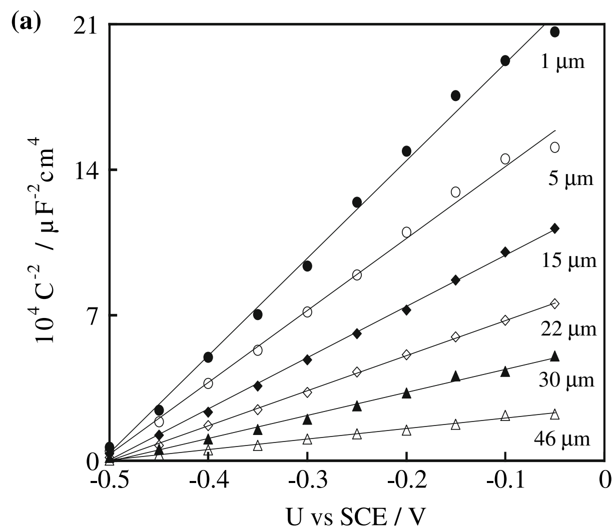

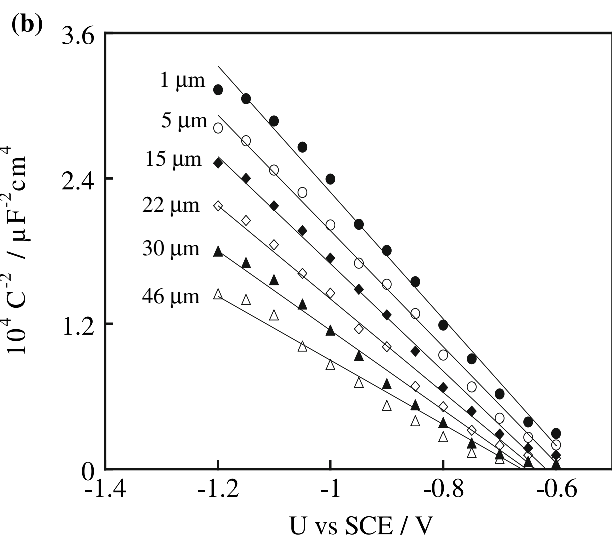

Fig. 4 Plots of C^{-2} versus the applied potential U for the oxide films formed on AISI 304 stainless steel abraded with wet SiC paper of different grit size (**a**) in the high potential range (U > −0.5 V), (**b**) in the low potential range (U < −0.5 V)

it can be assumed that an equivalent model describes the electronic structure of the thermally grown oxide films. This explanation is supported by the analytical results obtained by Auger Electron Spectroscopy (AES) [42, 43]. The quantitative approach shows that the oxide film is chemically composed of an inner layer of chromium oxide and an outer layer of iron oxide.

The influence of surface roughness is clearly shown in Fig. 4 by the quantitative variation of capacitance with grit size. The increase can be related to the influence of the space charge region formed by applying the potential at the film/solution interface. The variation in the space charge region can be related to defect structure and inhomogeneities of the film which are generally governed by the formation conditions and, in particular; the surface state of the substrate. The influence of the variation in real electrode surface with surface roughness is not taken into account and not discussed in this work.

From the slope of the straight lines of the C^{-2} versus U plots in Fig. 4, the donor and acceptor densities of the n-type and p-type layers of the oxide films formed on the different rough surfaces can be estimated using the Mott–Schottky relation [2–6, 23–27].

$$\frac{1}{C_{sc}^2} = \frac{1}{C_H^2} + \frac{2}{\varepsilon\varepsilon_0 q N_q}\left(U - U_{fb} - \frac{kT}{e}\right) \quad (2)$$

where C_{sc} is the space charge layer capacitance, C_H is the Helmholtz capacitance, N_q represents the donor or acceptor density, ε is the dielectric constant of the oxide film, ε_0 is the vacuum permittivity, q is the elementary charge (+e for

electrons, −e for holes), k is the Boltzmann constant, T is the absolute temperature and U_{fb} is the flatband potential.

The donor (N_D) and acceptor (N_A) densities were determined using $\varepsilon = 12$ for the dielectric constant of both oxides. This value has often been used for the determination of the doping densities of chromium oxide [44, 45] and iron oxide [23–25]. Table 1 shows that the value of the donor and the acceptor densities decreases when the grit size decreases. The values of the donor densities N_D are lower than those of the acceptor densities N_A. This is related to the difference in space charge layer thickness developed by the outer iron oxide and the inner chromium oxide layer. These results are in good agreement with those obtained by analytical study using Auger Electron Spectroscopy (AES). In fact, the AES results show that the thickness of the outer iron oxide layer formed at the film/electrolyte interface is greater than that of the inner chromium oxide layer developed at the film/metal interface.

Identical values were found [13] for the donor concentration of passive films formed at 0.8 V, which is $N_D = 2.5 \times 10^{20}$ cm^{-3}. The donor dopant (Fe^{2+} ions) concentration is not far from the anion vacancies concentration, which is about 2×10^{19} cm^{-3} in iron passive films formed in borate buffer solution [46]. It is also apparent from the results that, if Fe^{2+} is the doping specie in the films the decrease in N_D with decrease in surface roughness of the film-substrate means an impoverishment in this species. Thus, the films formed on less rough substrate contain a larger amount of Fe^{2+} than those formed on rougher substrate. In other words, the variation of the doping values with surface roughness can be explained by the close relation between the surface state of the substrate (roughness, dislocation, defect structure, …) and the semiconductor disorder which influences the doping densities. Assuming that there is a direct relationship between the thickness of the space charge layer and the open-circuit potential of the thermally grown oxide films, the results in Fig. 3 can be understood. As the space charge region of the outer layer of the film becomes thicker with decreasing grit size, a higher anodic polarisation will occur, which might account for the increase in the potential.

Table 1 Donor (N_D) and acceptor (N_A) densities for the n-type and p-type region of the oxide films

Grit size/µm	1	5	15	22	30	46
$N_D \times 10^{20}$/cm^{-3}	0.25	0.31	0.46	0.69	1.06	2.36
$N_A \times 10^{20}$/cm^{-3}	2.25	2.31	2.66	3.05	3.58	4.65

3.4 Frequency dependence of the capacitance

In order to investigate the influence of the frequency dependence on the capacitance results, measurements of the capacitance are performed at three different frequencies (3160 Hz, 1580 Hz and 316 Hz). The results presented in Fig. 5 concern measurements performed at applied potentials of 0 V and −1 V, respectively. These chosen potentials correspond to the development of the thicker space charge layer relative to the outer iron oxide layer and the inner chromium oxide layer, respectively. The influence of frequency dependence on the capacitance with variation in surface roughness via the grit size is clearly seen. In fact, it appears that for the less rough substrate corresponding to the small grit size value, the influence of the frequency dependence is practically negligible, i.e., no frequency dependence is manifested since all the values of the capacitance are approximately equal. The values exhibited by the capacitance C ≈ 2.5 µF cm^{-2} (Fig. 5a) and C ≈ 5.5 µF cm^{-2} (Fig. 5b) for the outer iron oxide layer and the inner oxide chromium layer respectively agree with the difference in the values of donor and acceptor densities presented in Table 1. The results presented in Fig. 5 show that the difference in the frequency dependence becomes greater with increasing grit size. In fact, the measured capacitance becomes increasively different as the grit size increases. This indicates that the frequency dependence influences the capacitance results in the same manner. Finally, the increases in capacitance, which promote a thinner space charge layer, agree with the difference of donor and acceptor densities presented in Table 1.

The frequency dispersion of capacitance has been reported in previous work on passive and oxide films [2]. This phenomenon has been attributed to the exponential variation of the resistivity as a function of the distance through the film [47]. Sato and all have also evoked the lack of three-dimensional long-range order due to small thickness of the films [48]. Some previous works [11, 49] attribute this phenomenon to the variable conductivity of the film due to variable stoichiometry and to non-uniform distribution of doping species across the film thickness. Finally, the dielectric relaxation phenomena due to the polar double layer contribution which leads to a complex dielectric constant [11, 50, 51] and the contribution of surface states to the capacitance response can also lead to the frequency dispersion phenomenon [52].

The frequency dispersion can be investigated by impedance measurements where the real and imaginary parts of the electric impedance Z are determined as a function of the frequency f over a wide range 10^{-3}–10^{5} Hz. The classical Bode representation ($\log Z = \beta \cdot \log f$), where β is a coefficient allowing the investigation of the frequency dispersion. The coefficient β can be related to the impedance of the

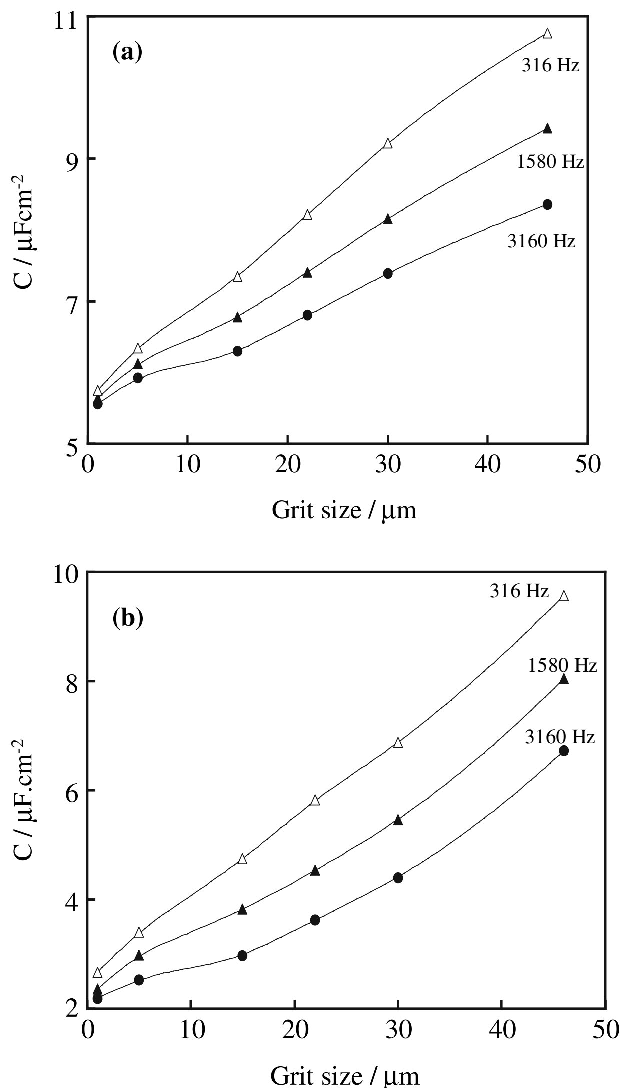

Fig. 5 Plots of C versus grit size for oxide films formed on AISI 304 stainless steel (**a**) at U = 0 V, (**b**) at U = −1 V

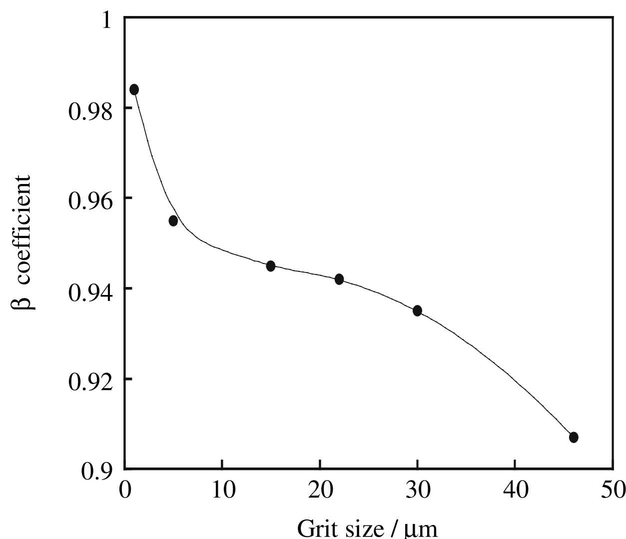

Fig. 6 Plot of β coefficient versus grit size for oxide films formed on AISI 304 stainless steel

constant phase element, Q, by $Z_Q = k(j2\pi f)^{-\beta}$, where k, is a constant. The phase element Q behaves as an ideal capacitor for $\beta = 1$ and an ideal resistance for $\beta = 0$. If $\beta = 0.5$, a Warburg element, which is often associated with semi-infinite diffusion, results [51]. Although no complete physical explanation of β can be given, this coefficient can be used for a comparative study of the frequency dependence. The variation of this coefficient as a function of grit size is represented in Fig. 6, and can be discussed in relation with the previous results of Fig. 5. In fact, the oxide film formed on less rough substrate corresponding to small grit size, present practically no frequency dispersion and the β coefficient, which tends to 1, reveals ideal capacitor behaviour. In these conditions, the thickness of the space charge layer becomes greater. The semiconducting properties of the oxide film are very close to those of a perfect crystalline semiconductor characterised by no frequency dispersion. On increasing the grit size, the coefficient, β, decreases, with consequent frequency dispersion. This confirms that the frequency dispersion of the capacitance measurements is strongly dependent on the nature of the film in terms of defects and nonstoichiometry. The films with low doping concentration exhibit less frequency dispersion. Since the β coefficient values range between 0.9 and 1, the equivalent circuit representing the oxide film/electrolyte system is far from that of an ideal resistor ($\beta = 0$) or a Warburg element ($\beta = 0.5$).

3.5 Photocurrent measurements

Assuming that, in the case of the films under study, the contribution to the photocurrent of the hole-electron pair formed in the bulk region is negligible, the quantum efficiency, η, defined as the ratio between the photocurrent, I_{ph}, and the incident photon flux, ϕ_0, of energy, $h\nu$, is given by the following relationship [53, 54]:

$$\eta = \frac{I_{ph}}{\phi_0} = qAw\frac{(h\nu - E_g)^n}{h\nu} \tag{3}$$

where A is a constant, q the elementary charge, w the thickness of the space charge layer and E_g the band gap energy. The exponent, n, depends on the type of transition between valence band and conduction band. Analysis of photocurrent spectra obtained with passive and oxide films shows that n = 2 is the most appropriate value to represent the photoelectrochemical behaviour according to Eq. 3. This value of n corresponds to indirect transitions in crystallised solids and non-direct transitions in amorphous

materials [55, 56]. Figure 7, where $(\eta h\nu)^{1/2}$ is plotted against hν, depicts the influence of grit size ranging from 1 μm to 46 μm, on the photoresponse spectra obtained for the oxidised 304 stainless steel. The results show that the quantum efficiency increases with decreasing grit size. These results agree with the fact that the number of donors presents in the external layers of the films decreases when grit size increases (Table 1) and can be associated to an enlargement of the space charge layer, corresponding to a weak value of the capacitance, in the oxide films. This can be explained if it is assumed that a decrease in the donor density corresponds to a diminution of film defects and the electron-hole recombination processes are favoured by the defects in the film. Extrapolating of $(\eta h\nu)^{1/2}$ to $h\nu = 0$, a threshold energy value around 2.3 eV is obtained whatever the nature of the film. This value is in excellent agreement with the reported band gap values of passive and oxide films formed on stainless steels and Fe–Cr alloys [2, 8, 9, 15, 56–58]. As clearly seen from this figure, the absorption edge position does not depend on the surface roughness of the film. Another feature of spectra presented in Fig. 7 is that the photoresponse evolution near absorption edge is not a sharp one, and shows sub-gap absorption. This phenomenon is the well-known band tail, traditionally associated with crystalline defects, impurities, deep levels or localised states in band-gap, when significant photocurrents were observed with sub-bandgap illumination. Figure 7 shows the existence of a photocurrent peak situated at 1.9 eV, e.g. for photon energies lower than E_g (in the sub-band gap region). This peak can be associated to transitions from valence band to the second donor level localised in the band gap. In fact, taking into account that

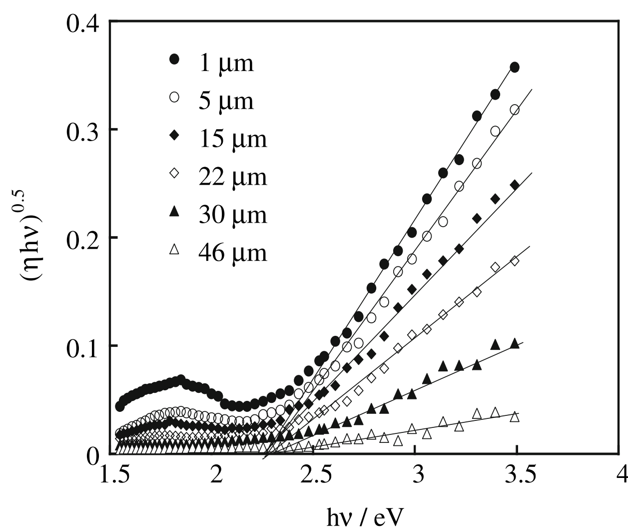

Fig. 7 Plots of $(\eta h\nu)^{0.5}$ versus the incident energy light, hν, for oxide films formed on AISI 304 stainless steel abraded with wet SiC paper of different grit size

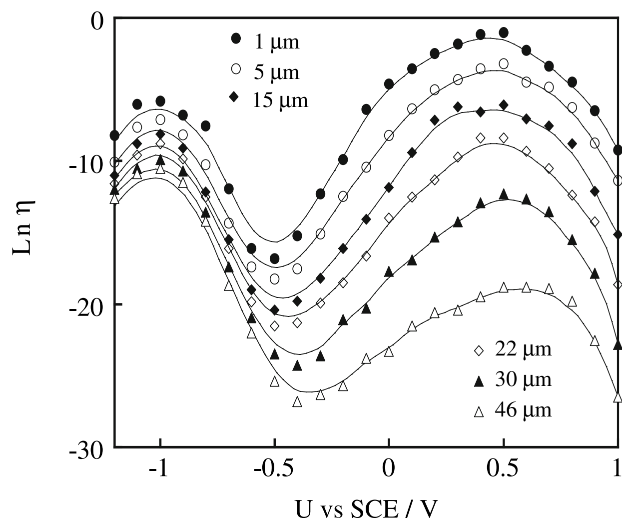

Fig. 8 Plots of Ln(η) versus the applied potential U for the oxide films formed on AISI 304 stainless steel abraded with wet SiC paper of different grit size

the band gap energy is 2.3 eV, it can be easily established [15, 56–58] that this level is situated at 0.4 eV below the conduction band. This interpretation supports the analysis of C^{-2} versus U plots observed in previous works [8, 27, 59, 60].

At fixed wavelength and variable potential, the photoresponse becomes governed by the variation in the band bending created by electrochemical polarisation and reflects the behaviour of the space charge layer under illumination. Experimentally, this kind of information can be obtained only if the incident light energy is greater than the band gap energy. At $\lambda = 370$ nm, where the photocurrent spectra present maximum intensity, the photocurrent was measured as a function of applied potential U and plots of ln(η) versus U were obtained (Fig. 8). They reflect the characteristic dependence of the depletion layer thickness on the potential and are analogous to Mott–Schottky behaviour. This is especially noticeable for all films in the case of potentials higher than −0.5 V, whereas, for potentials lower than this value, only thicker films reveal the same features. In thin films, the quantum efficiency is too low to be detected by this kind of measurements.

4 Conclusion

The influence of surface roughness on the electronic structure of oxide films formed at 350 °C on AISI 304 priory abraded with wet SiC paper of different grit size is demonstrated. Qualitatively, all the films reveal equivalent capacitance and photoelectrochemical behaviour, in spite of the fact that they are formed on different rough substrate. Quantitatively the decrease in photocurrent and the

increase in both capacitance and doping densities with increase grit size can be related to the formation of more disordered oxide films. In all cases, the semiconducting properties of the oxide films are governed by those of the outer iron oxide layer and the inner chromium oxide layer which are of n-type and p-type respectively. The electronic structure of the films is comparable to that of a p–n heterojunction due to the development of space charge layers in the outer iron oxide region at the film/electrolyte interface and in the inner chromium oxide region at the film/metal interface.

References

1. MacDonald DD, Sikora E, Sikora J (1996) Electrochim Acta 41:783
2. Hakiki NE, Montemor MF, Ferreira MGS, Da Cunha Belo M (2000) Corros Sci 42:687
3. Montemor MF, Ferreira MGS, Hakiki NE, Da Cunha Belo M (2000) Corros Sci 42:1635
4. Da Cunha Belo M, Walls M, Hakiki NE, Corset J, Picquenard E, Sagon G, Nöel D (1998) Corros Sci 40:447
5. Da Cunha Belo M, Rondot B, Compere C, Montemor MF, Simöes AMP, Ferreira MGS (1998) Corros Sci 40:481
6. Hakiki NE, Boudin S, Rondot B, Da Cunha Belo M (1995) Corros Sci 37:1809
7. Di Paola A, Di Quarto F, Sunseri C (1986) Corros Sci 26:935
8. Ferreira MGS, Hakiki NE, Goodlet G, Faty S, Simöes AMP, Da Cunha Belo M (2001) Electrochim Acta 46:3767
9. Da Cunha Belo M, Hakiki NE, Ferreira MGS (1999) Electrochim Acta 44:2473
10. Simöes AMP, Ferreira MGS, Lorang G, Da Cunha Belo M (1991) Electrochim Acta 36:315
11. Di Paola A (1989) Electrochim Acta 34:203
12. Hakiki NE, Da Cunha Belo M, Simöes AMP, Ferreira MGS (1999) J Electrochem Soc 146:807
13. Hakiki NE, Da Cunha Belo M, Simöes AMP, Ferreira MGS (1998) J Electrochem Soc 145:3821
14. Schmuki P, Virtanen S, Isaacs HS, Ryan MP, Davenport AJ, Böhni H, Stenberg T (1998) J Electrochem Soc 145:791
15. Hakiki NE, Da Cunha Belo M (1996) J Electrochem Soc 143:3088
16. Schmuki P, Bohni H (1992) J Eleclrochem Soc 139:1908
17. Simöes AMP, Ferreira MGS, Rondot B, Da Cunha Belo M (1990) J Electrochem Soc 137:82
18. Sunseri C, Piazza S, Di Quarto F (1990) J Electrochem Soc 137:2411
19. Schmuki P, Bohni H (1989) J Electrochem Soc 139:7
20. Sunseri C, Piazza S, Di Paola A, Di Quarto F (1987) J Electrochem Soc 134:2410
21. Hakiki NE, Da Cunha Belo M (1995) CR Acad Sci Paris 320(II):613
22. Hakiki NE, Da Cunha Belo M (1993) CR Acad Sci Paris 317(II):457
23. Delnick FM, Hackermann N (1979) J Electrochem Soc 126:732
24. Azumi K, Ohtsuka T, Sato N (1987) J Electrochem Soc 134:1352
25. Stimming U, Schultze JW (1976) Ber Bunsenges Phys Chem 8:129
26. Stimming U (1987) Langmuir 3:423
27. Dean MH, Stimming U (1987) J Electroanal Chem 228:135
28. Gillot B, Rousset A (1986) J Solid State Chem 65:322
29. Tapping RL, Davidson RD, McAlpine E, Lister DH (1986) Corros Sci 26:563
30. Lister DH, Davidson RD, McAlpine E (1986) Corros Sci 27:113
31. Robertson J (1991) Corros Sci 32:443
32. Kim YJ (1995) Corrosion 51:849
33. Schuster E, Neeb KH, Ahlanger W, Henkelmann R, Jarnstrom RTJ (1988) J Nucl Mater 152:1
34. Farrow RL, Benner RE (1983) Proc Electrochem Soc 83:190
35. Tjong SC (1983) Mater Res Bull 18:157
36. Fabis P, Heidersbach R, Brown C, Rockeh T (1981) Corrosion 37:700
37. Johnston C (1990) Vib Spectrosc 1:87
38. Oblonsky LJ, Devine TM (1995) Corros Sci 37:17
39. Derek J, Gardiner C, Littleton J, Bowden M (1988) Appl Spectrosc 42:15
40. Szklarska-Smialowska Z, Chou C, Kuo-Chin D, Xia Z, Zaizhu A (1991) Corros Sci 32:609
41. Xia Z, Lai WK, Szklarska-Smialowska Z (1991) Corrosion 47:173
42. Lorang G, Da Cunha Belo M, Simões AMP, Ferreira MGS (1994) J Electrochem Soc 141:3347
43. Simoes AMP, Ferreira MGS, Lorang G, Da Cunha Belo M (1991) Electrochim Acta 36:315
44. Lovrecek B, Sefaja J (1972) Electrochim Acta 17:1151
45. Mahla E, Nielsen N (1948) J Electrochem Soc 93:1
46. Sukhotin AM, Grilikhes MS, Lisovaya EV (1989) Electrochim Acta 34:109
47. Young L (1955) Trans Farad Soc 51:1250
48. Sato N, Kudo K Noda T (1971) Electrochim Acta 16:1909
49. Sholt JA, Van Geel Ch (1953) Philips Rev Rep 8:47
50. Dutoit EC, Van Meirhaeghe RL, Cardon F, Gomes WP (1975) Ber Bensenges Phys Chem 79:1206
51. Van Meirhaeghe RL, Dutoit EC, Cardon F, Gomes WP (1975) Electrochim Acta 20: 995
52. Macdonald JR (1987) Impedance spectroscopy. Wiley, NY
53. Gärtner WW (1959) Phys Rev 116:84
54. Butler MA (1977) J Appl Phys 48:1914
55. Pankove JI (1975) Optical processes in semiconductors. Dover, NY
56. Bube RH (1967) Photoconductivity of solids. Wiley, NY
57. Hakiki NE, Simöes AMP, Ferreira MGS, Da Cunha Belo M (2000) Port Electrochim Acta 18:113
58. Montemor MF, Ferreira MGS, Hakiki NE, Da Cunha Belo M (1998) Mater Sci Forum 289:1139
59. Hakiki NE, Da Cunha Belo M (1995) CR Acad Sci Paris 320(II):463
60. Kennedy JH, Frese KW (1987) J Electrochem Soc 125:723